Supplement of Geosci. Model Dev., 18, 9349–9384, 2025 https://doi.org/10.5194/gmd-18-9349-2025-supplement © Author(s) 2025. CC BY 4.0 License.





Supplement of

A process-based modeling of soil organic matter physical properties for land surface models – Part 1: Soil mixture theory

Bertrand Decharme

Correspondence to: Bertrand Decharme (bertrand.decharme@meteo.fr)

The copyright of individual parts of the supplement might differ from the article licence.

Section S1 Soil porosity as volumetric arithmetic mixing of each components

We now demonstrate how Equation (16), which expresses total soil porosity as a function of the bulk and solid densities of the composite soil system, leads to the arithmetic mixing formulation of Equation (17). Starting from Equation (16), we rewrite the expression as a single rational form and group the terms by component:

$$w_{sat} = \frac{\left(\frac{m_{om}}{\rho_{b_{om}}} + \frac{m_{ms}}{\rho_{b_{ms}}}\right) - \left(\frac{m_{om}}{\rho_{s_{om}}} + \frac{m_{ms}}{\rho_{s_{ms}}}\right)}{\left(\frac{m_{om}}{\rho_{b_{om}}} + \frac{m_{ms}}{\rho_{b_{ms}}}\right)} = \frac{\left(\frac{m_{om}}{\rho_{b_{om}}} - \frac{m_{om}}{\rho_{s_{om}}}\right) + \left(\frac{m_{ms}}{\rho_{b_{ms}}} - \frac{m_{ms}}{\rho_{s_{ms}}}\right)}{\left(\frac{m_{om}}{\rho_{b_{om}}} + \frac{m_{ms}}{\rho_{b_{ms}}}\right)}$$
(S1)

We then factor each component:

$$w_{sat} = \frac{\frac{m_{om}}{\rho_{b_{om}}} \left(1 - \frac{\rho_{b_{om}}}{\rho_{s_{om}}}\right) + \frac{m_{ms}}{\rho_{b_{ms}}} \left(1 - \frac{\rho_{b_{ms}}}{\rho_{s_{ms}}}\right)}{\left(\frac{m_{om}}{\rho_{b_{om}}} + \frac{m_{ms}}{\rho_{b_{ms}}}\right)}$$
(S2)

$$= \left(1 - \frac{\rho_{b_{om}}}{\rho_{s_{om}}}\right) \frac{\frac{m_{om}}{\rho_{b_{om}}}}{\left(\frac{m_{om}}{\rho_{b_{om}}} + \frac{m_{ms}}{\rho_{b_{ms}}}\right)} + \left(1 - \frac{\rho_{b_{ms}}}{\rho_{s_{ms}}}\right) \frac{\frac{m_{sm}}{\rho_{b_{ms}}}}{\left(\frac{m_{om}}{\rho_{b_{om}}} + \frac{m_{ms}}{\rho_{b_{ms}}}\right)}$$
(S3)

15 Using volume mixing from equation Equations (12c) and the mass-volume relationships from Equation (13c), we obtain:

$$w_{sat} = \left(1 - \frac{\rho_{b_{om}}}{\rho_{s_{om}}}\right) \frac{v_{b_{om}}}{(v_{b_{om}} + v_{b_{ms}})} + \left(1 - \frac{\rho_{b_{ms}}}{\rho_{s_{ms}}}\right) \frac{v_{b_{ms}}}{(v_{b_{om}} + v_{b_{ms}})}$$
(S4)

And then:

$$w_{sat} = \left(1 - \frac{\rho_{bom}}{\rho_{s_{om}}}\right) \frac{v_{bom}}{v_b} + \left(1 - \frac{\rho_{b_{ms}}}{\rho_{s_{ms}}}\right) \frac{v_{b_{ms}}}{v_b} \tag{S5}$$

which corresponds to Equation (17) of the manuscript.

20 Section S2 Liu and Lennartz (2019) k_{sat} pedotransfer function

Lennartz and Liu (2019) proposed a specific PTF for peats based on a reanalysis of a large secondary database from Liu and Lennartz (2019), using dry bulk density as the main predictor. The relationship expresses saturated hydraulic conductivity as a function of the dry bulk density of peats, r_{breat} (g·cm⁻³), as follows:

$$\log_{10}(k_{sat}) = \begin{cases} -17.01 \cdot r_{b_{peat}} + 2.19 & \forall r_{b_{peat}} \le 0.2 \text{ g} \cdot \text{cm}^{-3} \\ -1.21 & \forall 0.2 < r_{b_{peat}} \le 1.0 \text{ g} \cdot \text{cm}^{-3} \end{cases}$$
(S6)

25 where $\log_{10}(k_{sat})$ is expressed in cm.h⁻¹.

Section S3 Additional table

Table S1. Examples of typical hydraulic and thermal parameter values used in land surface models for organic soils. Thermal properties are generally based on Farouki (1981), while hydraulic parameters are derived from Letts et al. (2000) or Boelter (1966).

	Parameters and Definitions		Lawrence and Slater (2008)	Decharme et al. (2016)
$\overline{C_{s_{om}}}$	soil solid heat capacity	$(J.m^{-3}.K^{-1})$	2.5×10^6	2.5×10^{6}
$\lambda_{s_{om}}$	thermal conductivity of soil matrix	$(W.m^{-1}.K^{-1})$	0.25	0.25
$\lambda_{dry_{om}}$	dry thermal conductivity	$(W.m^{-1}.K^{-1})$	0.05	0.05
$w_{sat_{om}}$	porosity	$(m^3 \cdot m^{-3})$	0.9	0.93 to 0.845
b_{om}	pore-size distribution index	(-)	2.7	2.7 to 12
$\psi_{sat_{om}}$	air-entry pressure head	(m)	-0.0103	-0.0103 to -0.0101
$k_{sat_{om}}$	saturated hydraulic conductivity	$(m.s^{-1})$	1×10^{-4}	2.8×10^{-4} to 1×10^{-7}

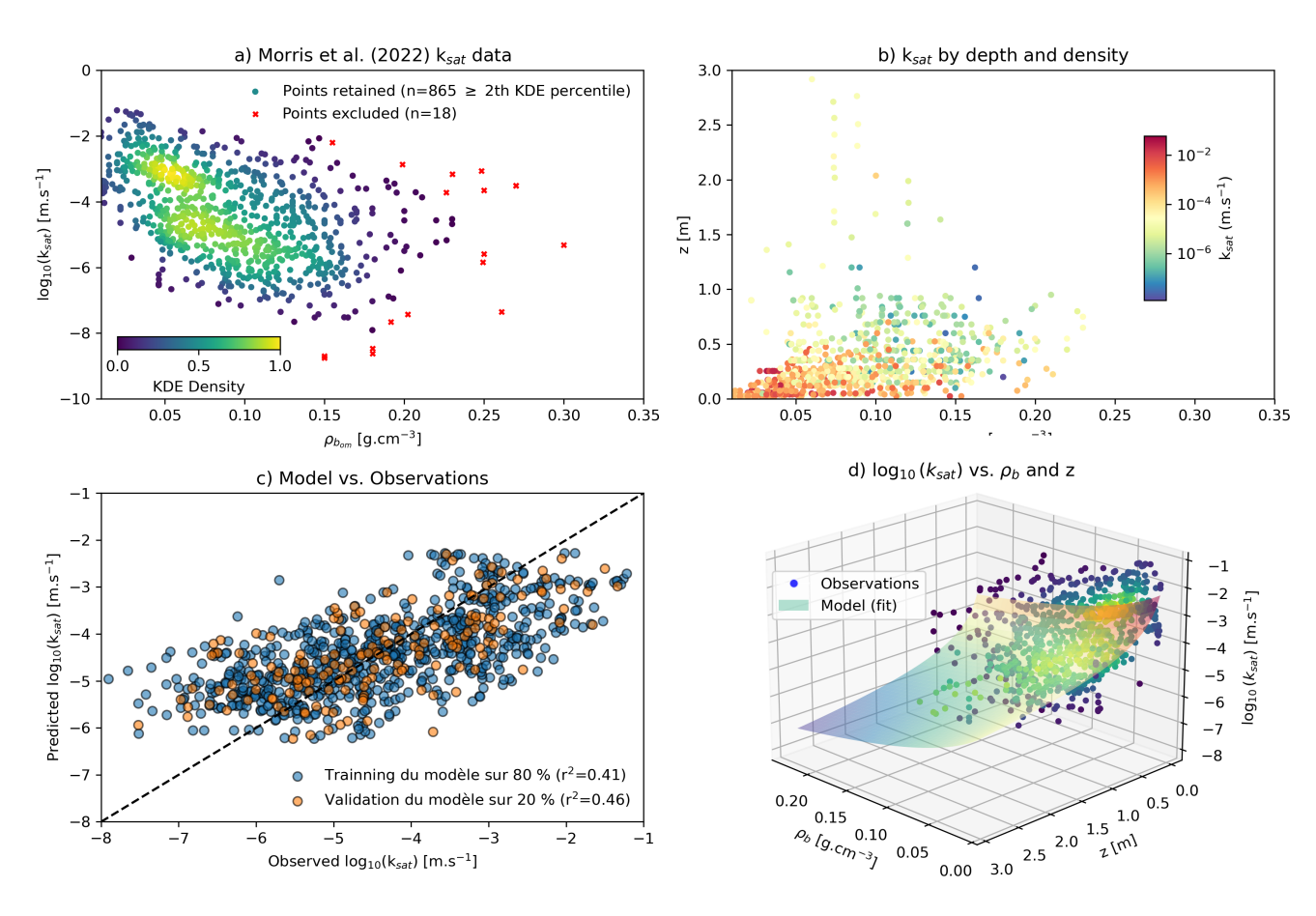


Figure S1. Multi-panel illustration of the data analysis and model development used to derive the pedotransfer function (PTF) for saturated hydraulic conductivity of organic matter $(k_{sat_{om}})$. (a) Density-based filtering of the dataset from Morris et al. (2022) using a 2D kernel density estimator (KDE) in the $[\rho_{b_{om}}, \log_{10}(k_{sat_{om}})]$ space. Data points with KDE values below the 2nd percentile (red crosses) were excluded as outliers, retaining 98% of the original dataset (865 points). (b) Scatter plot of $k_{sat_{om}}$ as a function of both depth (z) and organic bulk density, showing a general decline with increasing depth and density. (c) Comparison between model predictions and observations of $\log_{10}(k_{sat_{om}})$ for training (80%) and validation (20%) datasets. Coefficients of determination (r^2) are 0.41 and 0.46, respectively. (d) 3D visualization of the fitted model (Equation 36) showing the combined influence of depth and ρ_{bom} on $k_{sat_{om}}$, compared with the observations.

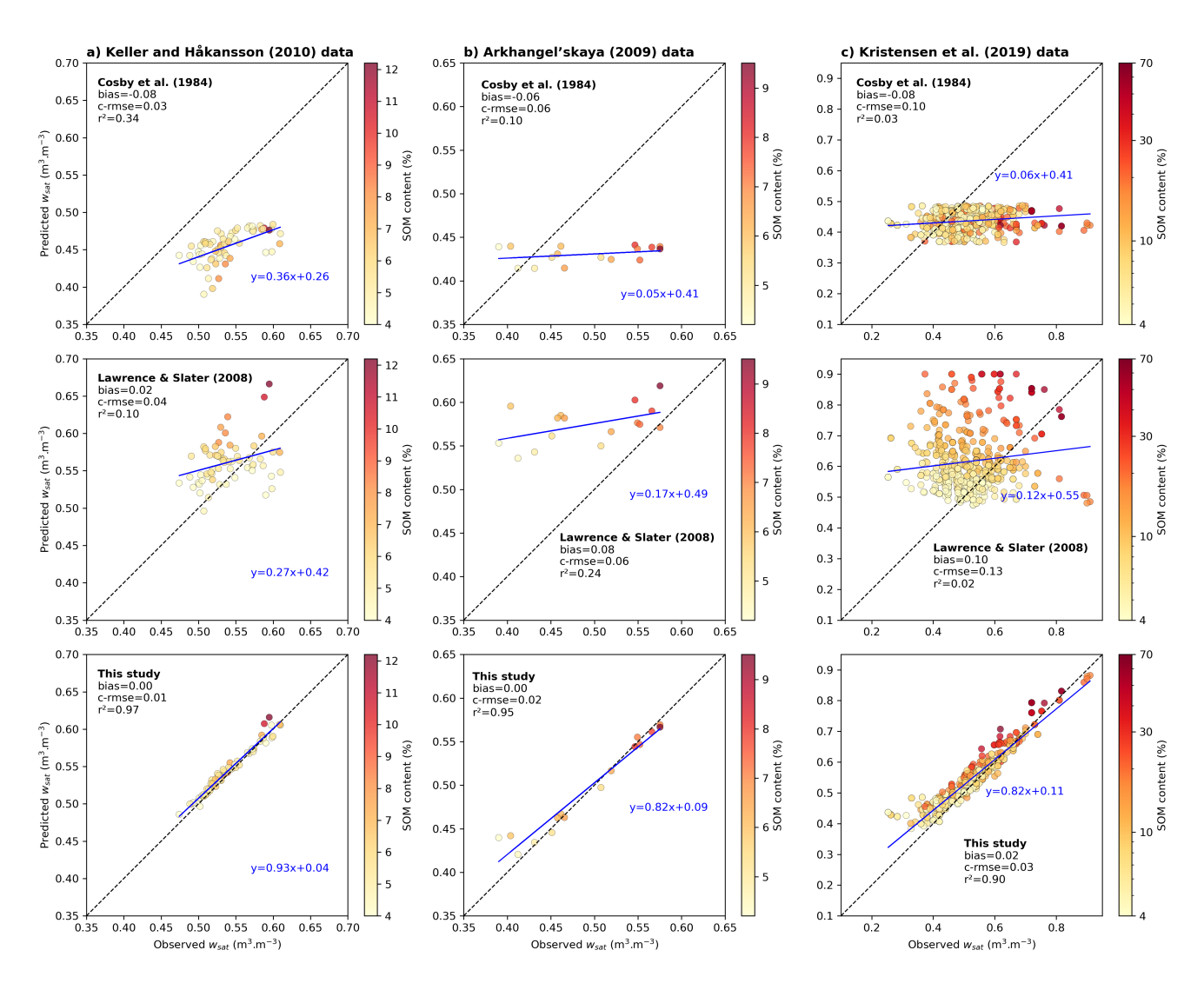


Figure S2. Same as Figure 4, but restricted to samples with $f_{m_{om}} \ge 4\%$ in the datasets of Keller and Håkansson (2010) and Kristensen et al. (2019), or with $f_{m_{oc}} \ge 2\%$ in the dataset of Arkhangel'skaya (2009).

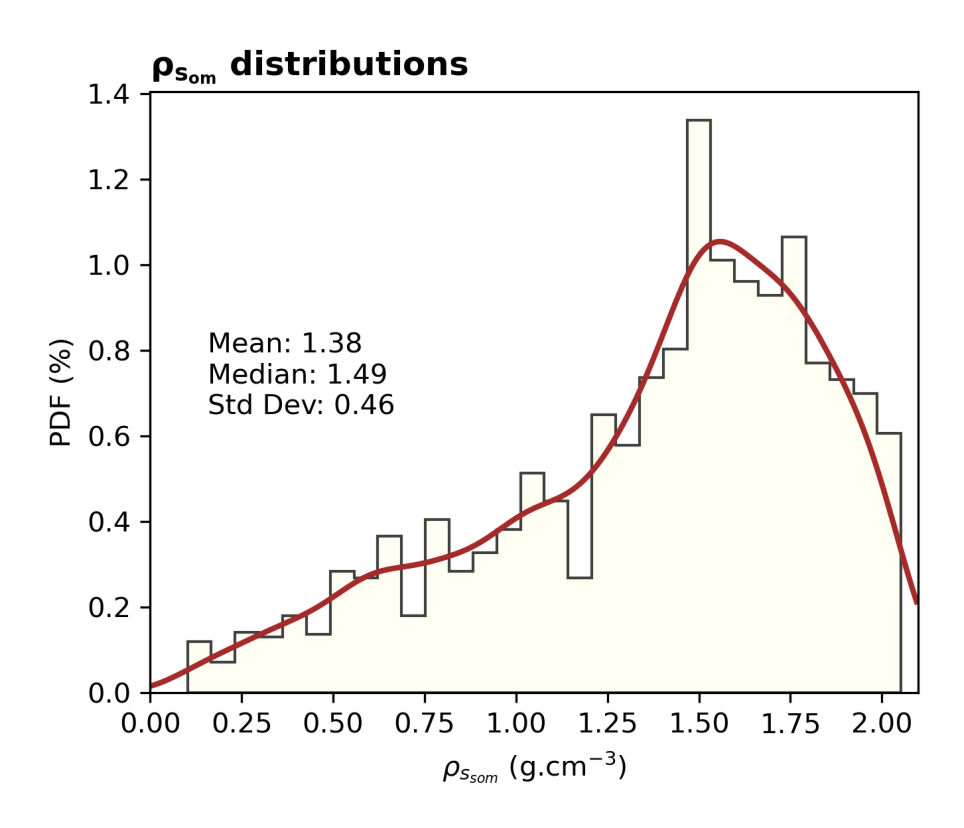


Figure S3. Distribution of organic matter particle density ($\rho_{s_{om}}$, g cm⁻³) across the compiled datasets. The histogram (bars) is shown with a kernel density estimate (red line). The mean, median, and standard deviation are indicated in the panel.

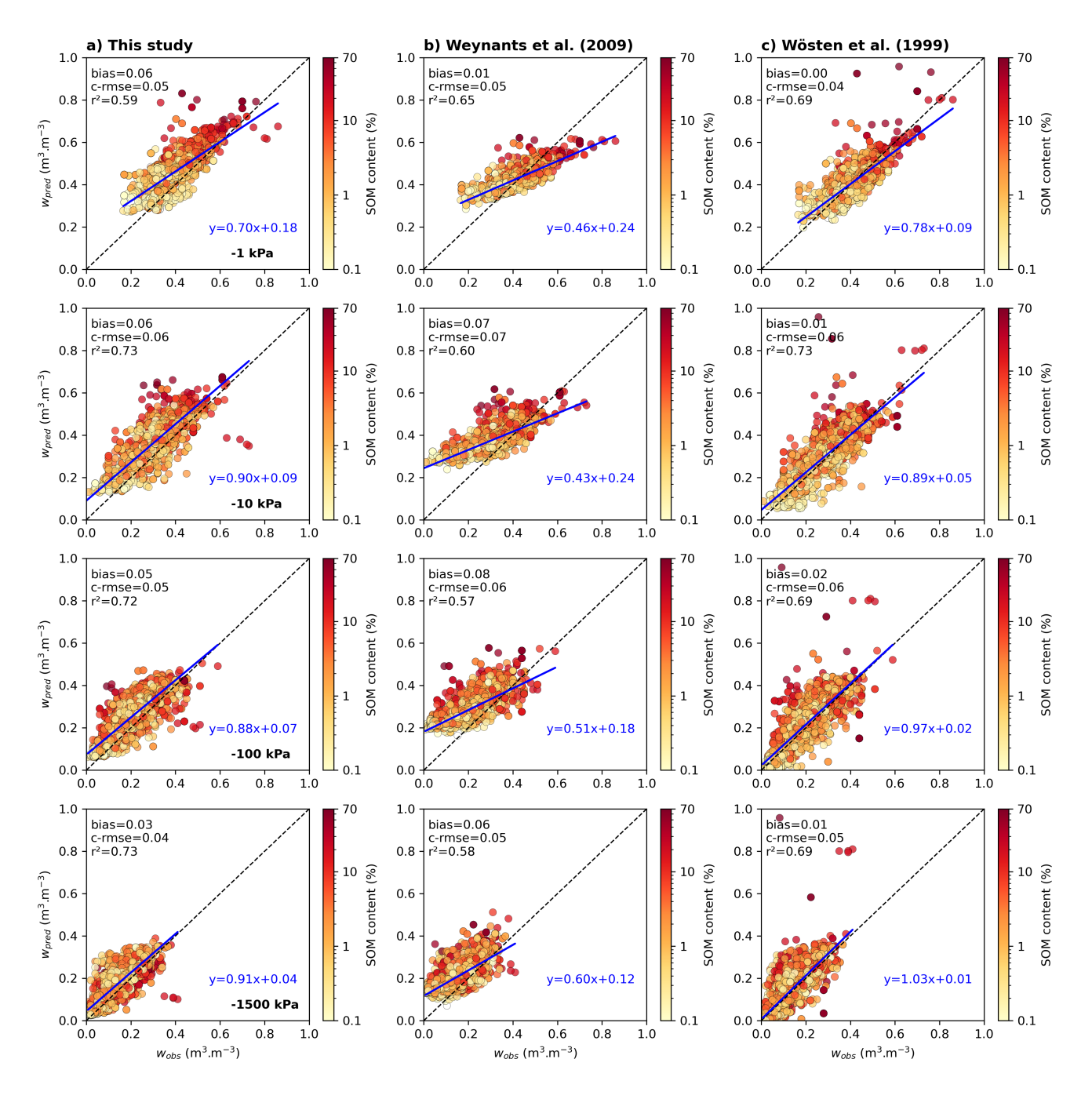


Figure S4. As Figure 6, but including the comparison of the PTFs of Weynants et al. (2009) and Wösten et al. (1999) with the dataset from Kristensen et al. (2019). Panels show the predicted versus observed volumetric water content at different matric potentials (-1, -10, -100, and -1500 kPa) for (a) this study, (b) Weynants et al. (2009), and (c) Wösten et al. (1999).

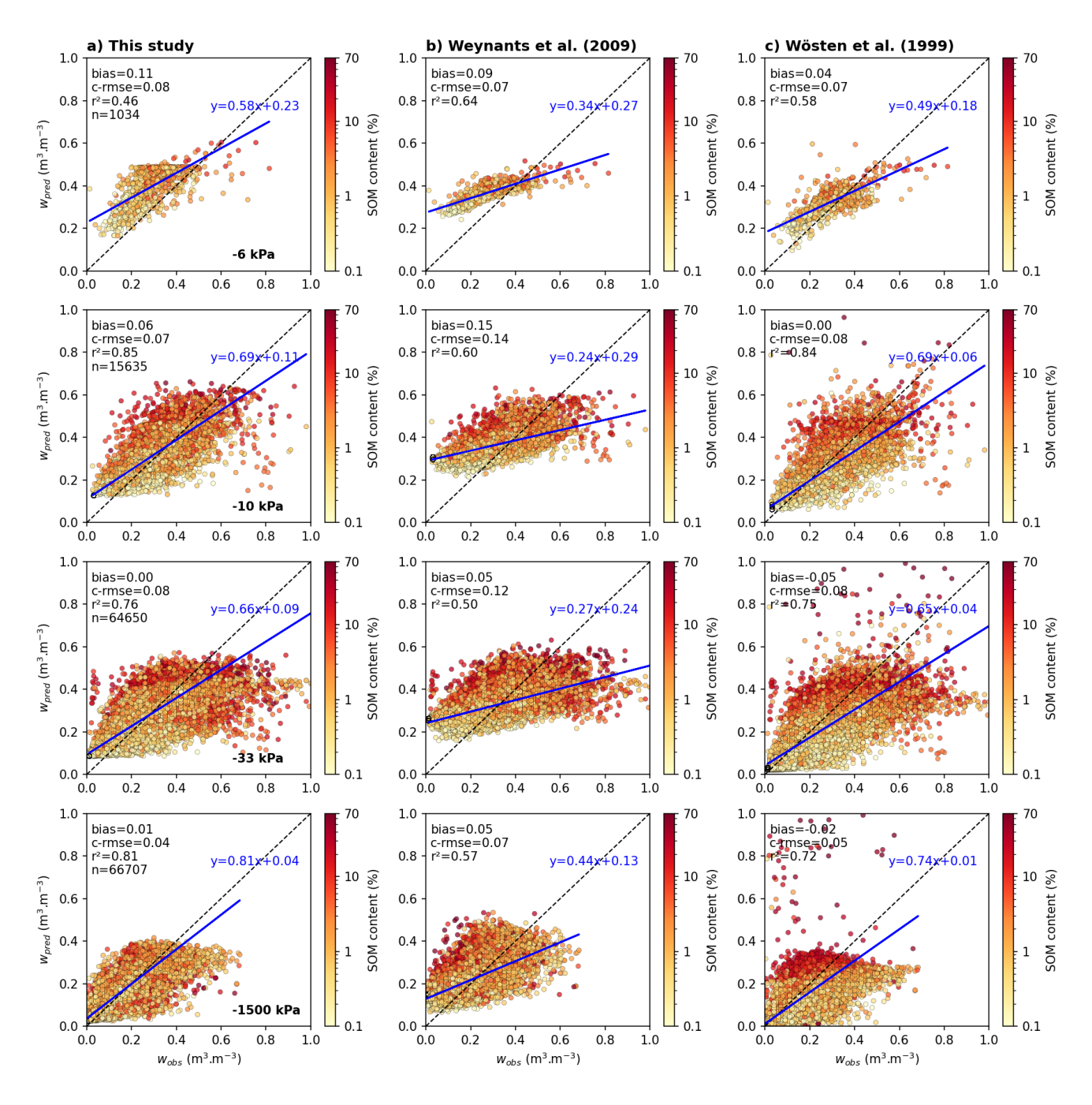


Figure S5. As Figure 7, but including the comparison of the PTFs of Weynants et al. (2009) and Wösten et al. (1999) with the dataset from Gupta et al. (2021). Panels show the predicted versus observed volumetric water content at different matric potentials (-6, -10, -33, and -1500 kPa) for (a) this study, (b) Weynants et al. (2009), and (c) Wösten et al. (1999).

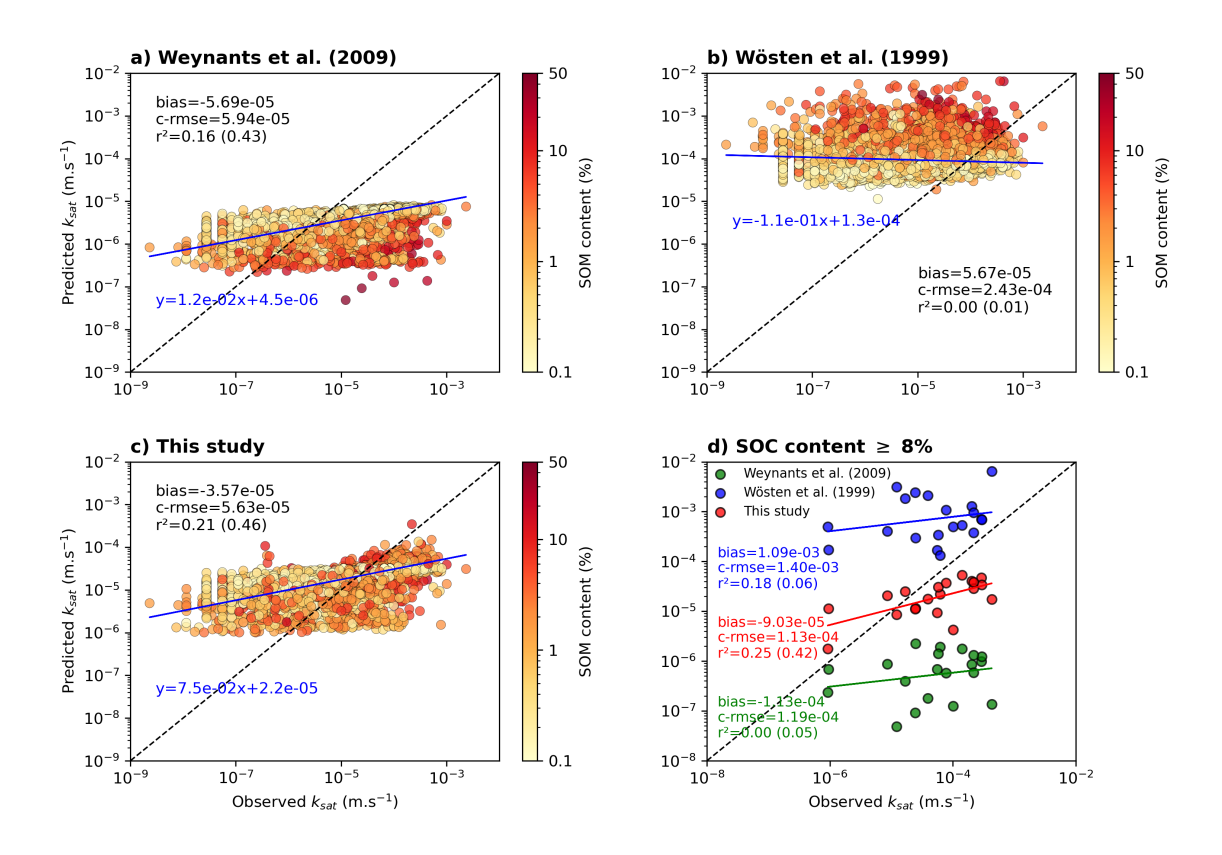


Figure S6. As Figure 8, but including the comparison of the PTFs of Weynants et al. (2009) and Wösten et al. (1999) with the dataset from Gupta et al. (2021). Panels show the predicted versus observed saturated hydraulic conductivity for (a) Weynants et al. (2009), (b) Wösten et al. (1999), (c) this study, and (d) soils with SOC content $\geq 8\%$.

References

50

- Arkhangel'skaya, T. A.: Parameterization and mathematical modeling of the dependence of soil thermal diffusivity on the water content, Eurasian Soil Science, 42, https://doi.org/10.1134/S1064229309020070, 2009.
 - Boelter, D. H.: Important Physical Properties of Peat Materials, Proceedings, third international peat congress, 1966.
 - Decharme, B., Brun, E., Boone, A., Delire, C., Le Moigne, P., and Morin, S.: Impacts of snow and organic soils parameterization on northern Eurasian soil temperature profiles simulated by the ISBA land surface model, Cryosphere, 10, https://doi.org/10.5194/tc-10-853-2016, 2016
- Farouki, O. T.: Thermal Properties of Soils CRREL Monograph, US Army Cold Regions Research and Engineering Laboratory, 11, https://usace.contentdm.oclc.org/digital/collection/p266001coll1/id/6302, 1981.
 - Gupta, S., Hengl, T., Lehmann, P., Bonetti, S., and Or, D.: SoilKsatDB: Global database of soil saturated hydraulic conductivity measurements for geoscience applications, Earth System Science Data, 13, https://doi.org/10.5194/essd-13-1593-2021, 2021.
 - Keller, T. and Håkansson, I.: Estimation of reference bulk density from soil particle size distribution and soil organic matter content, Geoderma, https://doi.org/10.1016/j.geoderma.2009.11.013, 2010.
 - Kristensen, J. A., Balstrøm, T., Jones, R. J. A., Jones, A., Montanarella, L., Panagos, P., and Breuning-Madsen, H.: Development of a harmonised soil profile analytical database for Europe: a resource for supporting regional soil management, SOIL, 5, 289–301, https://doi.org/10.5194/soil-5-289-2019, 2019.
- Lawrence, D. M. and Slater, A. G.: Incorporating organic soil into a global climate model, Climate Dynamics, 30, https://doi.org/10.1007/s00382-007-0278-1, 2008.
 - Lennartz, B. and Liu, H.: Hydraulic functions of peat soils and ecosystem service, https://doi.org/10.3389/fenvs.2019.00092, 2019.
 - Letts, M. G., Comer, N. T., Roulet, N. T., Skarupa, M. R., and Verseghy, D. L.: Parametrization of peatland hydraulic properties for the Canadian land surface scheme, Atmosphere Ocean, 38, https://doi.org/10.1080/07055900.2000.9649643, 2000.
 - Liu, H. and Lennartz, B.: Hydraulic properties of peat soils along a bulk density gradient—A meta study, Hydrological Processes, 33, https://doi.org/10.1002/hyp.13314, 2019.
 - Morris, P. J., Davies, M. L., Baird, A. J., Balliston, N., Bourgault, M. A., Clymo, R. S., Fewster, R. E., Furukawa, A. K., Holden, J., Kessel, E., Ketcheson, S. J., Kløve, B., Larocque, M., Marttila, H., Menberu, M. W., Moore, P. A., Price, J. S., Ronkanen, A. K., Rosa, E., Strack, M., Surridge, B. W., Waddington, J. M., Whittington, P., and Wilkinson, S. L.: Saturated Hydraulic Conductivity in Northern Peats Inferred From Other Measurements, Water Resources Research, 58, https://doi.org/10.1029/2022WR033181, 2022.
- Weynants, M., Vereecken, H., and Javaux, M.: Revisiting Vereecken Pedotransfer Functions: Introducing a Closed-Form Hydraulic Model, Vadose Zone Journal, 8, https://doi.org/10.2136/vzj2008.0062, 2009.
 - Wösten, J. H. M., Lilly, A., Nemes, A., and Le Bas, C.: Development and use of a database of hydraulic properties of European soils, Geoderma, https://doi.org/10.1016/S0016-7061(98)00132-3, 1999.